Regular and Chaotic Transport in Asymmetric Periodic Potentials: Inertia Ratchets

P. Jung

Center For Complex Systems Research, Beckman Institute, and Department of Physics, University of Illinois, Urbana, Illinois 61801

J. G. Kissner and P. Hänggi

Institut für Physik, Universität Augsburg, Memminger Strasse 6, D-86135 Augsburg, Germany

(Received 29 November 1995)

Motivated by recent work on stochastic ratchets, we consider the effect of finite inertia onto the directed motion in a deterministically rocked, periodic potential lacking reflection symmetry. Characterizing the motion by cumulants of the contracted, time-dependent solution of the Liouville equation, we can distinguish regular from chaotic transport. The first cumulant describes a stationary current that exhibits multiple reversals versus increasing driving strength, whereas the second cumulant yields a measure for its variance. Chaotic transport exhibits universal (Gaussian) scaling behavior. [S0031-9007(96)00064-6]

PACS numbers: 82.20.Mj, 05.40.+j, 05.45.+b

It is generally appreciated that—in accordance with the second law of thermodynamics—usable work cannot be extracted from equilibrium fluctuations. Devices and phenomena that are only in apparent contradiction with this second law have been discussed by Feynman, Leighton, and Sands [1] and even much earlier in the heyday of Brownian motion by Smoluchowski [2]. In the presence of nonequilibrium forces the situation changes drastically. Then, directed transport of Brownian particles in asymmetric periodic potentials (ratchets) can be induced by the application of nonthermal forces [3–8] or with the help of deterministic, periodic coherent forces [4,9,10]. These nonequilibrium models recently gained much interest in view of their role in describing the physics of molecular motors [5,6] and their potential for novel technological applications on nanoscales and microscales [11]. The previous literature on these schemes is characterized by the limitation of using an overdamped ratchet dynamics throughout. A particular challenge thus presents the study of finite inertia for the ratcheting mechanism in the absence of thermal and nonthermal forces. With finite inertia, the dynamics is allowed to become more complex, exhibiting both regular and chaotic behavior. Using the model of a periodically rocked ratchet, we shall investigate the mutual interplay of regular and chaotic dynamics for directed transport, in particular, to what extent deterministically induced chaos mimics the role of noise. In doing so, we use novel diagnostic tools, such as the behavior of cumulant averages for the phase-space probability, whose time evolution is governed in the deterministic limit by a dissipative, nonautonomous Liouvillian. Nonstationary effects, such as the broadening of the phase-space probability—a measure for the fluctuations of the net-flux (on a coarse grained scale)—are taken into account by not applying periodic boundary conditions.

As a working model, we use an underdamped particle, periodically driven in an asymmetric periodic potential,

$$\epsilon\ddot{x}(t) + \dot{x}(t) = -\frac{d}{dx}V_\mu(x) + A\sin(\Omega t)\,, \qquad (1)$$

with the potential shown in Fig. 1 (see also [10])

$$V_\mu(x) = -\sin(x) - \mu\sin(2x)\,. \qquad (2)$$

All variables in (1) and (2) are scaled dimensionless and μ is set to $\mu = 1/4$ throughout this work.

We first briefly discuss the case of massless particles ($\epsilon = 0$), i.e., overdamped motion. The motion is bound for driving amplitudes $A < A_0(\Omega)$; i.e., the solution of Eq. (1) approaches a function which is periodic in time for large times. For $A_0(\Omega) < A$, the motion can become unrestricted. The average velocity assumes an asymptotic value (that is independent of the initial conditions) of the form

$$v_{nm} = \frac{x(t + nT) - x(t)}{nT} = \frac{m}{n}\Omega\,, \qquad (3)$$

with integers m and n. A direct consequence of the overdamped motion is that the net flux is directed towards the shallow side of the ratchet (positive current), i.e., $m, n > 0$ in Eq. (3). For finite mass ϵ, the situation is

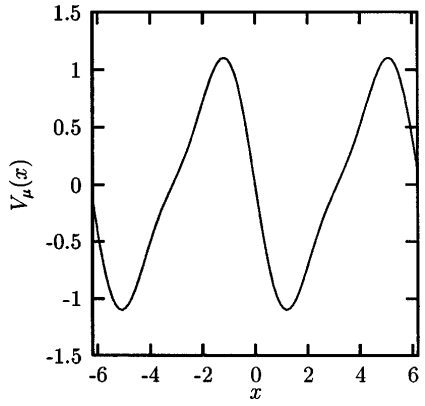

FIG. 1. The ratchet potential $V_\mu(x) = -\sin(x) - \mu\sin(2x)$ for $\mu = 1/4$, as used in the text.

 0031-9007/96/76(18)/3436(4)$10.00

different. The trajectories described by (1) can become chaotic; i.e., the trajectories are erratic on a time scale large against the largest Liapunov coefficient and the net flux can go in both directions. This raises the key question studied in this paper: How does intrinsic chaotic motion resemble noise driven motion in ratchets?

Equation (1) has a variety of solutions which can be obtained by numerical integration. We are using their transport properties as a classification criterion. Regular trajectories are described by $x(t + nT) = x(t) + 2\pi m$ with $n \in \mathcal{N}$ and $m \in \mathcal{Z}$. Regular, nontransporting trajectories are being characterized by tuples $(n, m = 0)$. Regular, transporting solutions are characterized by the tuples $(n, m \neq 0)$. These trajectories are periodic with period n (subharmonic for $n > 1$) on a toroidal phase space obtained by using periodic boundary conditions; i.e., x is identified with $x + 2\pi$. In contrast to the overdamped case the transport can now be due to the inertia in either direction; i.e., the average velocity can assume the values given in Eq. (3) with $m = 0, \pm 1, \pm 2, \ldots$. Given a fixed set of parameters, it is important to note that—depending on the initial conditions—different classes of trajectories have been observed by numerical simulation. For example, at $A = 0.624, \Omega = 0.1, \epsilon = 20$, asymptotic trajectories are either periodic, (1,0), or current carrying, $(2, -1)$. This situation calls for interesting technological applications, since it allows for the separation of particles starting with different initial conditions (a detailed discussion will be published elsewhere [12]).

A third class is chaotic trajectories. Their behavior has been studied by numerically simulating the time evolution of an initial probability density in $(x, \dot{x})$ space (see below for details). For $\Omega = 0.1, \epsilon = 20$, and those values of A in $0 < A < 10$, where the system is living on a chaotic attractor, there was always a net drift to the right or to the left; i.e., particles move on average either to the left or to the right. The chaotic attractor can be observed in a stroboscopic plot in $(x, \dot{x})$ space after mapping the unbounded dynamics in space onto one period of the potential, i.e., $x(t) \rightarrow x(t) \,(\mathrm{mod} 2\pi)$. We did not observe coexisting chaotic attractors in our working model (1). For chaotic maps with periodic forces, the onset of diffusive behavior caused by the memory loss due to chaotic dynamics has been studied some time ago [13].

By integrating Eq. (1) numerically, one realizes that the drift of a single chaotic trajectory exhibits strong fluctuations. An appropriate tool for describing transport is therefore a time-dependent probability measure. Given the initial probability density $\rho_0(x, \dot{x}, t)$, its time evolution is given by

$$\rho(x, \dot{x}, t) = \int dx' \int d\dot{x}' \, \delta(x - x_d(x', \dot{x}', t)) \times \delta(\dot{x} - \dot{x}_d(x', \dot{x}', t)) \, \rho_0(x', \dot{x}') \,. \quad (4)$$

Here $x_d(x', \dot{x}', t)$ is the solution of (1) with initial conditions $x_d(t = 0) = x'$ and $\dot{x}_d(t = 0) = \dot{x}'$. In contrast to the conventional treatment, we do *not* apply periodic boundary conditions. This allows us to study the broadening of the probability density as a function of time [12].

As an example for the chaotic regime, we depict in Fig. 2(a) the time evolution of the contracted probability density $\bar{\rho}(x, t) = \int d\dot{x}' \, \rho(x, \dot{x}', t)$ for $A = 0.79, \Omega = 0.1, \epsilon = 20$ and $\mu = 1/4$. The x axis has been partitioned so that one partition ranges over one period of the potential. The initial probability density was chosen Gaussian with a width of $1/2$ in space and $\dot{x}(t = 0) = 0$. On a short time scale the probability density becomes more complicated, but approaches asymptotically a Gaussian shape; cf. Fig. 2(b). Because we are not interested in time scales of a single period, where one observes the oscillatory contribution of the driving force, we switch to a coarse grained description by looking at the system stroboscopically ($t = nT = 2\pi n/\Omega$). Time t will therefore denote these stroboscopic times. In Fig. 3, we show the first and second cumulants of the probability density as a function of time. Apart from initial transients, we observe a linear mean and a linear variance—typical for Brownian motion. The third cumulant and higher cumulants contain more of the detailed structure of the density, and are therefore more

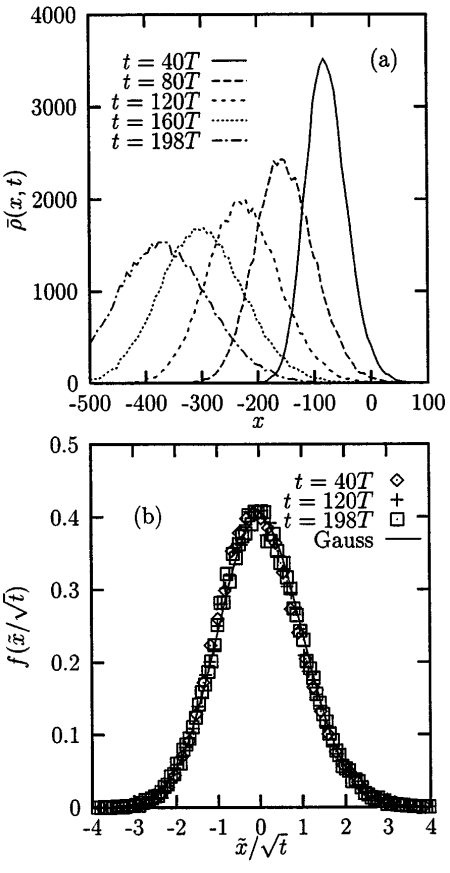

FIG. 2. Snapshots of the probability density, obtained by simulating 50 000 trajectories, are shown in (a) for $A = 0.79, \Omega = 0.1$, and $\epsilon = 20$. The universal, normalized scaling function $\bar{p}(\tilde{x}, t)$, Eq. (7), obtained from the same densities is shown in (b).

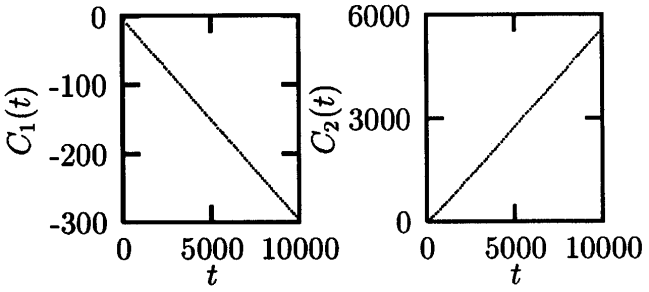

FIG. 3. The first two cumulants $C_1(t)$ and $C_2(t)$ for $A = 0.79, \Omega = 0.1$, and $\epsilon = 20$ are shown stroboscopically as a function of time ($t_n = nT$).

complicated functions of time. As a common feature we find that their modulus increases slower than $t^{3/2}$.

Based on the observations above, we will show in the following that the probability density will become *effectively Gaussian.* Thus the first and second cumulants are sufficient to describe the time evolution and transport.

The characteristic function $\Phi(s) = \langle \exp[-isx(t)] \rangle$ of the contracted probability density $\bar{\rho}(x,t)$ is written in terms of its cumulants $C_k(t)$ as

$$\Phi(s) = \exp\left(-isC_1(t) - \frac{1}{2} s^2 C_2(t) + \sum_{k=3}^{\infty} \frac{(-is)^k}{k!} C_k(t) \right). \tag{5}$$

Making use of the numerically observed behavior for large times, i.e., $C_1(t) = vt$, and $C_2(t) = \sigma^2 t$ as $t \to \infty$, we can analyze the long time behavior of the probability density. First, we introduce the integration variable $u = s\sqrt{t}$, and define the relative position $\tilde{x} = x - vt$. The scaled probability density $\bar{p}(\tilde{x},t) = \bar{\rho}(x,t)$ can then be written as

$$\bar{p}(\tilde{x},t) = \frac{1}{\sqrt{t}} \int_{-\infty}^{\infty} \exp\left[iu \frac{\tilde{x}}{\sqrt{t}} - \frac{1}{2} \sigma^2 u^2 \right] \times \exp\left[\sum_{k=3}^{\infty} \frac{(-iu)^k}{k!} t^{-k/2} C_k(t) \right] du\,. \tag{6}$$

In the scaling limit $t \to \infty$ with $\tilde{x}/\sqrt{t}$ kept constant, the terms $C_{k\geq 3}(t)$ in the second exponential become irrelevant (this, of course, relies on the observation that for $k \geq 3$ $C_k/t^{k/2} \to 0$ as $t \to \infty$).

The first two terms, which are relevant in the scaling limit, describe a Gaussian density with the scaling form $t^{-1/2} f(\tilde{x}/\sqrt{t})$, while the other terms describe corrections to it. With the knowledge of all coefficients, those corrections to scaling can be obtained by expanding the second exponential, leading to an asymptotic expansion of $\bar{p}$,

$$\bar{p}(\tilde{x},t) = \frac{1}{\sqrt{t}} f\left(\frac{\tilde{x}}{\sqrt{t}}\right) \left[1 + t^{-3/2} C_3(t) h\left(\frac{\tilde{x}}{\sqrt{t}}\right) + \cdots \right], \tag{7}$$

where h is an analytic function describing the leading correction to scaling, and $f(y) = \exp(-y^2/2\sigma^2)$. Therefore, for large times, the probability density approaches a shape which allows rescaling to a (universal) Gaussian distribution; see Fig. 2(b). The long time evolution does not depend on the choice of the initial probability. It is interesting to compare $\bar{p}(\tilde{x},t)$ to the time-dependent probability density of a Brownian particle in a symmetric periodic potential (see, e.g., in [14]). For large times it shows, apart from the vanishing drift, the scaling form (7).

In case of a single regular attractor, i.e., all trajectories are regular and obey $x(t + nT) = x(t) + 2\pi m$ with the same tuple (n,m), the probability density for large times approaches a positive normalized function of the form $\bar{\rho}(x, t \to \infty) = f(x - vt)$ with $v = m\Omega/n$. The characteristic function of $f(x - vt)$, given by $\phi(v,s) = \exp(-ivts)\phi_0(s)$, where $\phi_0(s)$ is time independent, implies a first cumulant $C_1(t) = vt$ and constant higher cumulants $C_{k\geq 2}$ (see Fig. 4). For nontransporting regular attractors, i.e., $v = 0$, all cumulants are time independent, corresponding to a stationary probability density. We remind the reader that the time scale t is actually a coarse grained time scale, on which periodic variations of the probability density within nT are not visible.

In the case of coexisting regular attractors different trajectories, corresponding to different sets (n_1, m_1) and (n_2, m_2), are drifting with different average velocities $v_1 = m_1\Omega/n_1$ and $v_2 = m_2\Omega/n_2$, respectively. The probability density consists of several moving peaks with constant widths each (for large times), but generally different velocities, $v_2 \neq v_1$. The cumulant generating function, $g(s) = \ln \phi(s) = \ln[\exp(-iv_1ts)\phi_0^{(1)}(s) + \exp(-iv_2ts)\phi_0^{(2)}(s)]$ yields cumulants of the form $C_k(t) \propto t^k$. The first cumulant is again linear in time, i.e., $C_1(t) = \alpha t = (Av_1 + Bv_2)t$, where A and B are the relative weights of the two coexisting attractors. The second cumulant $C_2(t)$ is, in contrast to the cases above, quadratic in time. Such a case is realized, for example, with the parameter values $A = 0.624, \Omega = 0.1$, and $\epsilon = 20$.

With the above developed tools, we will now analyze the transport properties in the asymmetric periodic potential. In Fig. 5, we depict the current v as a function of the driving amplitude at $\epsilon = 20$. In the range $0 < A < 1.00$, where the overdamped system ($\epsilon = 0$)

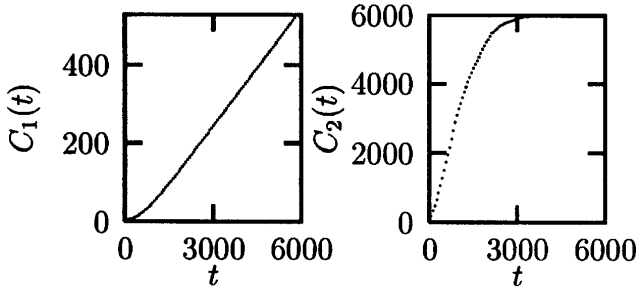

FIG. 4. The first two cumulants $C_1(t)$ and $C_2(t)$ for $A = 1.1, \Omega = 0.1$, and $\epsilon = 20$ are shown stroboscopically as a function of time ($t_n = nT$).

always exhibits either zero or positive current, we observe a variety of transport phenomena: in situations with zero transport, i.e., $v = 0$, the system has a single regular attractor with period $n = 1$. The transport in the interval $0.61 < A < 0.64$ is regular for most parts. In this region we find a negative current. Applying our diagnostic tools above, we conclude from the dependence $C_2(t) \propto t^2$ that there are coexisting regular attractors [15]. As a check, a stroboscopic plot yields a regular behavior that does not match with any of the values $v_{nm} = m\Omega/n$, because the transport is regular with contributions from several coexisting regular attractors. For $A > 0.7$, the motion is typically chaotic. As an example we show Fig. 3 ($A = 0.79$). The linear dependence of the first two cumulants as a function of time implies chaotic motion. This is confirmed by a stroboscopic plot. The transport is negative, which is towards the steep side of the potential (cf. Fig. 1), for all trajectories. At some parameters (e.g., $A = 0.615$), we observe behavior which resembles regular transport for small times, with a clear-cut transition to diffusive chaotic transport for large times (see [12] for a detailed discussion). For larger amplitudes $A > 1$, one finds regular regimes and chaotic regimes. The currents in the chaotic regimes are directed in either the positive or the negative direction. The linear time dependence of the first and second cumulants, the observation that the higher cumulants $C_{n\geq 3}(t)$ increase slower than $t^{3/2}$, and the resulting scaling laws, as presented above, apply in all tested cases in $A < 10$.

In summary, we have presented novel results for an inertia ratchet. The system can exhibit a current flow in either direction (multiple current reversals). The direction can be controlled by adjusting the amplitude of the external, periodic driving (cf. Fig. 5); furthermore, it depends sensitively on the strength of the inertia and friction [16]. This makes it especially interesting for technological applications. The system's dynamics is characterized by the time dependence of cumulants of the particle distribution. In the case of directed chaotic transport, the second cumulant is a measure for the intrinsic *current fluctuations,* and thus for the reliability of the ratchet mechanism. Our diagnostic tools allow a distinction between different forms of regular and chaotic transport; these enable a systematic description of chaos-induced currents in terms of a universal Gaussian scaling.

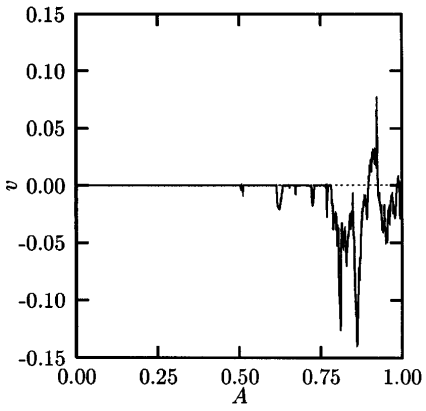

FIG. 5. The transport coefficient $v = \dot{C}_1(t \to \infty)$ is shown as a function of the driving amplitude A for $\epsilon = 20$ and $\Omega = 0.1$.

P.J. thanks the Deutsche Forschungsgemeinschaft for financial support within the Heisenberg program.

[1] R. P. Feynman, R. B. Leighton, and M. Sands, *The Feynman Lectures on Physics* (Addison-Wesley, Reading, MA, 1966), Vol. 1, Chap. 46.
[2] M. v. Smoluchowski, Phys. Z. **XIII**, 1069 (1912).
[3] A. Ajdari and J. Prost, C. R. Acad. Sci. Ser. II **315**, 1635 (1992).
[4] M. O. Magnasco, Phys. Rev. Lett. **71**, 1477 (1993).
[5] R. D. Astumian and M. Bier, Phys. Rev. Lett. **72**, 1766 (1994); R. D. Astumian and M. Bier, Biophys. J. **70**, 637 (1996).
[6] C. S. Peskin, B. Ermentrout, and G. Oster, *Cell Mechanics and Cellular Engineering,* edited by V. C. Mow *et al.* (Springer, New York, 1994).
[7] C. R. Doering, W. Horsthemke, and J. Riordan, Phys. Rev. Lett. **72**, 2984 (1994).
[8] J. Luczka, R. Bartussek, and P. Hänggi, Europhys. Lett. **31**, 431 (1995).
[9] A. Ajdari, D. Mukamel, L. Peliti, and J. Prost, J. Phys. I (France) **4**, 1551 (1994).
[10] R. Bartussek, P. Hänggi, and J. G. Kissner, Europhys. Lett. **28**, 459 (1994).
[11] J. Rousselet, L. Salome, A. Ajdari, and J. Prost, Nature (London) **370**, 446 (1994); L. P. Faucheux, L. S. Bourelieu, P. D. Kaplan, and A. J. Libchaber, Phys. Rev. Lett. **74**, 1504 (1995).
[12] P. Jung (to be published).
[13] S. Grossmann and H. Fujisaka, Phys. Rev. A **26**, 1779 (1982); Z. Phys. B **48**, 261 (1982); T. Geisel and J. Nierwetberg, Phys. Rev. Lett. **48**, 7 (1982); M. Schell, S. Fraser, and R. Kapral, Phys. Rev. A **26**, 504 (1982).
[14] H. Risken, *The Fokker-Planck Equation,* Springer Series in Synergetics (Springer-Verlag, Berlin, 1984), Sec. 11.7.2.
[15] Coexisting strange attractors would yield the same dependence to leading order, but we have not observed this case in our simulations.
[16] Setting the friction to zero, we obtain a nonergodic behavior. In particular, a stationary, nonzero current does no longer emerge. Hence, a finite, stationary current requires also a finite dissipation, see also [1].